Astron. Astrophys. 344, 991–1000 (1999)

ASTRONOMY AND ASTROPHYSICS

Analysis of the Geminid meteor stream, 1958–1997, from radar observations

P. Pecina and M. Šimek

Astronomical Institute of the Academy of Sciences of the Czech Republic, CZ-251 65 Ondřejov, Czech Republic

Received 16 September 1998 / Accepted 13 January 1999

Abstract. Results of long-term radar observations of the Geminids in the period 1958–1997 are presented. Mean activity profiles along the Earth's passage through the stream show a systematic change of the peak activity and the width of the stream depending on the distribution of echo durations across the stream. Faint particles are more concentrated in inner orbits while the large ones dominate in the outer orbits. A skewness of the activity profiles is evident for echo durations $T \geq 1$ s. The patterns of mass-distribution index s and of the flux are also presented. The activity levels of individual years show moderate scatter over the examined period except in 1995 when low activity of the sporadic background results in an apparent high activity of the shower.

Key words: meteors, meteoroids

1. Introduction

The Geminid meteor shower is one of the best known and most systematically observed in the northern hemisphere. The regular appearance of its high activity on 13–14 December is its main feature. The stream is also unique because of an extremely short orbital period of about 2.6 years. Its parent body was not known until the discovery of 3200 Phaeton which is generally accepted to be associated with the stream (Whipple 1983).

Observations of the Geminids have been performed regularly with the Ondřejov meteor radar since 1958 to 1997 except for 1970, 1972, 1979, 1983, and 1988. The shower has also been observed regularly by radar at the Springhill Observatory near Ottawa from 1957 to 1977. Both long-term sets of data were analyzed in a series of papers (Hajduk et al. 1974, McIntosh & Šimek 1980, Šimek & McIntosh 1989, and others) which resulted in the determination of cross-section shower activity patterns along the Earth's path through the stream on an hour-by-hour basis. The method of deconvolving the data from the radar diurnal sampling function – both the diurnal variation of the background, and the variation of shower hourly rates as a function of the elevation of the shower radiant, where the antenna receiving efficiency is derived from diurnal samples of observed hourly shower rates – has been described by Šimek (1985) and by Šimek & McIntosh (1986). Contrary to earlier studies expressed in arbitrary units, all parameters are here presented in absolute values of the mean shower and background rates.

Data from 35 annual observations, during which the parameters of the radar remained unchanged, cover 15 orbital periods of the stream. Shower activity profiles and some of their parameters are presented, as are shower flux profile, an analysis of mass-distribution across the stream and its diurnal variations, and yearly levels of the shower activity.

The course of activity levels of the sporadic background in individual years was compared with the variation of the solar activity cycle.

2. Equipment, methods and observations

The Ondřejov radar, located at $49°55'$N, $14°47'$E, operates at a frequency of 37.5 MHz with a pulse length of 10 μs, a peak power of 20 kW, and a repetition frequency of 500 Hz. The beam width of the antenna system is approximately $52°$ in the vertical plane and $36°$ in the orthogonal plane which is fixed at $45°$ elevation. The antenna is steerable in azimuth. For shower observations the beam is pointed to an azimuth differing by $180°$ from the azimuth of the relevant shower radiant. The radar records the meteor echoes on 35 mm film in a range-time format. Any influence on the observed count such as masking of echoes by electrical or atmospheric noise must be corrected for. As the same radiant-antenna geometry and technical parameters of the radar were maintained during all observations since 1958, the series of data is homogeneous enough to perform a long-term analysis. The duration of each echo longer than 0.4 s is measured with an accuracy of ± 0.05 s.

A method for generating the activity variation of the shower from observed echo rates and hence the dependence of the stream cross section on various effects (i.e. diurnal variation of recorded echo rates, antenna pattern, position of shower radiant, etc) was developed by Šimek (1985) and Šimek & McIntosh (1986). Later, the method was slightly refined to yield results in mean hourly rates. The input data are year, date and hour, limits of a particular echo duration class, net observing time within a particular hour, and number of recorded echoes in each hour,

Send offprint requests to: P. Pecina (ppecina@asu.cas.cz)

solar longitude, $L_\odot$ (Epoch 1950.0) on the first day of the observing period, equivalent $\triangle L_\odot$ corresponding to one hour, and the solar longitude limits of the shower and sporadic periods. When calculating the mean shower and mean background rates, records shorter than 30 minutes were not used for the analysis while the others were normalized to equivalent hourly rates. The output of the calculation yields the mean shower rate patterns across the stream, correction factors for the diurnal variation of the observed echo rates (inverse to the response function of the radar), diurnal variation of the mean background rates, levels of the shower activity (shower to background ratio), and the levels of the background activity for every year of observations. In the program input neither radar nor other parameters are included. The method is applicable under the following assumptions:

1) the cross-section activity patterns of an analyzed meteor shower are geometrically similar on a year-to-year basis and differ only by a multiplication factor;
2) the same condition is valid for the diurnal variation of the background rates;
3) all parameters of the radar remain constant over the whole analyzed period;
4) the sporadic background recorded immediately before and after the shower activity period remains the same also during the shower period.

We are here concerned with the counts of radar echoes in four classes of echo duration. The class divisions are $0.4 \leq T < 1.0$, $1.0 \leq T \leq 8$, $T \geq 1$, and $T > 8.0$ seconds.

The limiting sensitivity of the Ondřejov radar according to Znojil et al. (1981) is about +8.0 M_r where M_r designates the radio magnitude. We have analyzed in this work overdense meteor echo activity according to their durations with the lower limit of 0.4 s. The mass-distribution index, s, for overdense meteor echoes may be inferred either from the conventional formula (e. g. Kaiser 1955)

$$\log N_c = -\frac{3}{4}(s-1)\log T + \text{const.}, \quad (1)$$

where N_c is the cumulative number of echoes having durations at least T seconds, or from simultaneous determination of the flux, Θ_{m_0}, and s. From the theory it follows that Eq. (1) is valid when ambipolar diffusion is the only process acting inside the ionized meteor path. Jones et al. (1990) recognized two principal regions corresponding to different dissipative processes operating in the ionized trail. While diffusion alone is dominant for echoes of shorter duration appearing at greater heights in the atmosphere, longer echo durations from meteors at lower heights are controlled mainly by different chemical and physical processes resulting in expressions differing from the simple formula (1). The mass-distribution index, s, is then represented well by the slope of the initial linear portion of the $\log N_c$ vs. $\log T$ curve.

All recorded echoes having duration $T \geq 0.4$ s were considered for the calculation of the mass-distribution indices. When the observation lasted only a fraction of an hour, the same fraction of sporadic meteors determined for that particular hour and year was subtracted to obtain the number of shower meteors for this part of that hour. All shower meteors were then summarized for each hour within the selected range of solar longitudes, $L_\odot$, over all years. Cumulative echo counts were determined in 20 echo duration classes differing by $\triangle \log T \simeq 0.1$ in the interval $0.4 \leq T \leq 30$ s which covers the diffusion as well as chemistry regions of meteor echo occurrence. In all cases the diffusion region was well defined and separated from the chemistry region. A Geminid echo duration of 0.4 s corresponds to +3.5 M_r radio magnitude.

The flux determination has been based on the comparison of observed shower rates with the theoretical rates as expressed by the formula

$$N^{the}(t_1,t_2;T_1,T_2) = (s-1)m_0^{s-1}\Theta_{m_0}F(s;t_1,t_2,T_1,T_2) \quad (2)$$

(see Pecina 1982) for the simultaneous determination of cumulative flux, Θ_{m_0} (related to limiting mass $m_0 = 10^{-5}$ kg), as well as of the mass distribution index, s. Since $F(.)$ is represented by an integral, the values of $N^{the}(.)$ for longer intervals can be computed as the sum of the corresponding values valid for shorter intervals. This statement holds true with respect to both time and duration. The time dependence in $F(.)$ is due to the dependence of integration limits within the echo plane on configuration of the shower radiant (and consequently also the echo plane) and the antenna pattern.

Since it is not easy, from the point of view of numerical computation, to evaluate cumulative rates, the additive property of $F(.)$ with respect to duration allows computation of theoretical pseudo-cumulative rates in Eq. (2). The term pseudo-cumulative indicates that the integration with respect to the duration T in $F(.)$ is carried out over a finite interval $[T_i, T_L]$. The fixed right hand side limit of each interval, T_L, is common for all subintervals and equals 30 s in our case – compare the T-interval above. We would like to stress here that the function $F(.)$ takes into account the fact that the region within the echo plane contributing to $N^{the}(.)$ differs for different duration classes which is partly responsible for the nonlinearity of the whole $\log N$ vs $\log T$ curve. The second cause of its nonlinearity was allowed for by taking into account the attachment of trail free electrons to ozone molecules (Jones et al. 1990). An attachment constant of $a_e = 7 \times 10^{-18}\,\mathrm{m^3\,s^{-1}}$, has been employed (e. g. Baggaley 1972).

The parameters Θ_{m_0} and s have been determined from the least squares condition

$$\sum_{i=1}^{n}[N_i^{obs} - (s-1)m_0^{s-1}\Theta_{m_0}F(s;t_1,t_2,T_i,T_L)]^2 = \min, \quad (3)$$

where the index i enumerates the i-th duration interval $[T_i, T_L]$, and N_i^{obs} stands for the observed pseudo-cumulative rates. These have been computed from the usual cumulative ones by simply subtracting from them the rate corresponding to the interval $[T_L, \infty)$. Eq. (3) contains Θ_{m_0} as a linear quantity but this is not the case with respect to s. Therefore, we were forced to compute both quantities iteratively using the Newton-Gauss method.

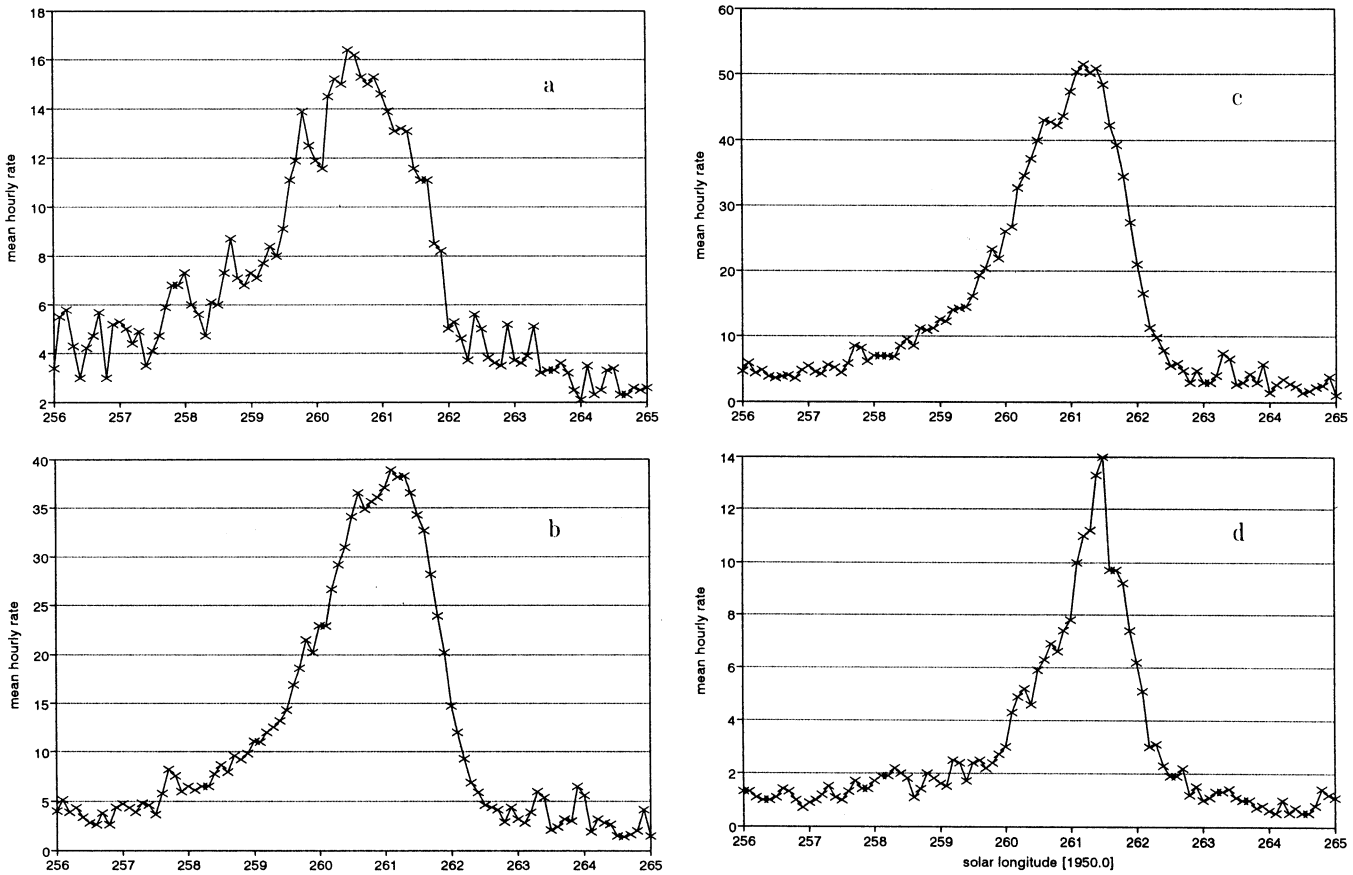

Fig. 1a–d. Mean hourly rates of Geminids 1958–1997, **a** class 1: $0.4 \leq T < 1.0$ s, **b** class 2: $1.0 \leq T \leq 8$ s, **c** class 3: $T \geq 1.0$ s, and **d** class 4: $T > 8.0$ s, as a function of solar longitude, $L_\odot$ (1950.0).

The function $F(.)$ depends also on some physical constants and functions. We have used the same ionization probability as Pecina (1982) did, i. e. $\beta = \beta_0 v^{3.5}$ with $\beta_0 = 1.26 \times 10^{-7}$ if v is expressed in km s^{-1} – see Kashcheev et al. (1967). Pecina (1982) used the ablation parameter $\sigma \simeq 0.06$ s^{2}km^{-2} and $K = A\Gamma\delta^{-2/3} \simeq 0.0295$ (in SI units). These values were taken from the work of Jacchia et al. (1965). However, since the appearance of this article new methods were developed which enabled the values of σ to be evaluated much more precisely. One of the most precise methods has been used by Spurný (1993) who has found that Geminids can be well represented by $\sigma \simeq 0.01$ s^{2}km^{-2} rather than by the value Pecina adopted in the past. This new σ-value, on the other hand, also forces the K-value to change. The above value of K would result in heights of Geminid echoes having duration $T = 0.4$ s such that they would correspond to ranges falling in the blocking gap and, consequently, they could not be observed by the Ondřejov radar. Hence, a value of K higher than that noted above was necessary. This value was found to be $K = 0.1103$, which followed from the demand that meteors with duration $T \simeq 0.7$–0.8 s should have the maximum ionization height of 93 km valid for Geminids (e. g. McKinley 1961). The further course of the work is based on these new values of the mentioned constants.

3. Activity profiles

The number of shower echoes which can be recorded by a radar depends on the relation of the observer's position on the Earth to the vector defining the motion of the stream particles. There is a strong diurnal variation determined by the time variation of the mutual position of the shower radiant and the radar antenna pattern. The shower counts are superimposed on the background of sporadic meteors which has its own strong diurnal variation. To determine the activity of shower meteors, one must subtract out the background counts and eliminate the diurnal variations. For details see Šimek (1985) and Šimek & McIntosh (1986). The method will be outlined only briefly here.

Because of the quarter-day shift in the diurnal cycle due to the leap-year effect, the underlying activity curve should be determined as a function of solar longitude, $L_\odot$, related to a fixed epoch. The epoch 1950.0 has been used in this paper for comparison with earlier results. After subtracting the background rates by means of a mean background model, the shower activity averaged over all the data is determined by the iterative technique of Šimek & McIntosh (1986) which was slightly adapted to obtain results in absolute instead of arbitrary units.

The results of the shower activity profile procedure are shown in Fig. 1 where shower activity is represented in shower mean hourly rates related to $\triangle L_\odot = 0^\circ\!.1$. The mean relative

Table 1. Geminid shower parameters in four echo duration classes. The following abbreviations have been used: edc – echo duration class in seconds, nes – number of echoes in the sample, rmr – radio magnitude range, slma – solar longitude at maximum activity, wp – width of the profile in degrees, sr – shape ratio (σ_b/σ_a), r – coefficient of correlation with R, r_{BL} – coefficient of correlation of the Bumba-Lindblad model. For an explanation of r and r_{BL}, see Sect. 4.

	Class 1	Class 2	Class 3	Class 4
edc	$0.4 \le T < 1.0$	$1.0 \le T < 8.0$	$T \ge 1.0$	$T > 8.0$
nes	18185	50314	59579	9741
rmr	$3.5 \le M_r < 2.8$	$2.8 \le M_r \le 0.6$	$M_r \ge 2.8$	$M_r > 0.6$
slma	260.55 ± 0.10	261.15 ± 0.12	261.25 ± 0.11	261.45 ± 0.10
wp	2.63 ± 0.05	2.16 ± 0.05	1.92 ± 0.04	1.11 ± 0.06
sr	0.95 ± 0.05	1.61 ± 0.10	2.05 ± 0.10	1.31 ± 0.16
r	0.95 ± 0.03	0.83 ± 0.09	0.87 ± 0.08	0.96 ± 0.02
r_{BL}	-0.92 ± 0.04	-0.75 ± 0.13	-0.78 ± 0.12	-0.91 ± 0.05

Table 2. Positions of the shower peak activity. Positions of the peak activity of the shower for different echo duration classes (in seconds) are listed in the first row. The second row contains the corresponding radio magnitude M_r at the center of the duration class with the last value of M_r estimated from Fig. 1 in Šimek (1987). The third row presents the solar longitude in degrees (Epoch 1950.0) of the positions of the peak activity.

0.4–0.5	0.6–0.8	0.9–1.2	1.3–1.7	1.8–2.5	2.6–3.5	3.6–4.6	4.7–6.0	6.1–10.0	> 10.0
3.45	3.10	2.75	2.40	2.05	1.70	1.35	1.05	0.60	-0.60
260.60	260.55	260.55	260.80	261.05	261.05	261.30	261.25	261.35	261.50

standard deviation is close to $3\,\%$ of the relevant value. Other shower parameters, namely: number of shower echoes in the sample, radio magnitude range, solar longitude at the maximum activity, width of the stream, w, measured at the half-amplitude points related to the shape factor σ_b/σ_a by $w = \sigma_b + \sigma_a$, where σ_b is the portion of w before $L_{\odot_{max}}$, and σ_a is the portion after $L_{\odot_{max}}$, are presented in Table 1. The radio magnitude, M_r, was calculated using Eq. (4) derived by Šimek (1987) for the Geminids in the form

$$M_r = 2.77\text{–}2.08 \log T - 0.39(\log T)^2. \quad (4)$$

In our study of the relation between sporadic background rates and solar activity r represents the correlation index between solar relative number, R, and sporadic background levels. The quantities r and r_{BL} are discussed in Sect. 4.

The change of positions of the peak activity is remarkable feature of the Geminid stream which has been shown already by several authors. For its better definition, the location of maximum activity was determined for 10 groups of echo duration each of them containing about 9000 echoes. The result is given in Table 2 and Eq. (5).

The observation that the Geminid maximum activity of faint meteors preceded the others was already found by Plavcová (1965), McIntosh & Šimek (1980), and others. Concentration of faint particles in the inner parts of the stream is apparent. This is usually attributed to the Poynting-Robertson effect shifting the orbits of small particles towards the sun. Fox et al. (1983) have also noted the skewness of the Geminids and explained it on the basis of gravitational and planetary perturbations during the dynamic evolution of the stream. They suppose a symmetrical cross-section for the period 1962–1982 changing for the last two decades in the century to a similar skewness which we observed in classes 2–4 of our observations. The effect from the forty years span of our observations is indicated in Eq. (5), by the least-squares fit of $L_{\odot_{max}}$ vs. M_r in Table 2.

Table 3. Diurnal variations of the mean inverse value of the response function. Diurnal variations of the mean inverse value of the radar response function for four echo duration classes of the Geminids listed in Table 1, as a function of the radiant zenith distance, z_R, referring to the elevation angle of the reflecting point at the main vertical plane of the antenna beam, at the center of the observed one-hour interval. Presented values correspond to the multiplication factor which converts observed hourly rates for the Geminid radiant position to mean hourly shower rates. Since the antenna pattern varies with the hilly configuration of the terrain surrounding the radar, the values of the (response function)$^{-1}$ for identical values of z_R depend on the azimuth angle of the antenna beam center, A, which is also presented.

$z_R[^\circ]$	$A[^\circ]$	class 1	class 2	class 3	class 4
18	157	1.13 ± 0.07	0.89 ± 0.10	0.88 ± 0.10	0.95 ± 0.08
18	198	1.00 ± 0.06	0.87 ± 0.09	0.88 ± 0.10	1.09 ± 0.10
23	231	0.86 ± 0.05	0.92 ± 0.10	0.94 ± 0.10	1.38 ± 0.12
24	126	1.06 ± 0.07	1.02 ± 0.11	0.99 ± 0.11	1.12 ± 0.10
32	251	1.17 ± 0.07	1.24 ± 0.13	1.23 ± 0.14	1.38 ± 0.12
32	108	1.29 ± 0.08	1.56 ± 0.17	1.46 ± 0.16	1.31 ± 0.11
41	265	1.71 ± 0.11	1.99 ± 0.22	1.81 ± 0.20	1.57 ± 0.14
42	94	1.40 ± 0.09	1.94 ± 0.21	1.82 ± 0.20	1.50 ± 0.13
51	276	1.83 ± 0.11	2.76 ± 0.30	2.63 ± 0.29	2.00 ± 0.18
51	82	1.50 ± 0.09	2.41 ± 0.26	2.51 ± 0.28	2.13 ± 0.19
61	287	2.45 ± 0.15	4.15 ± 0.45	3.53 ± 0.39	2.03 ± 0.18
61	72	1.89 ± 0.12	2.88 ± 0.31	2.88 ± 0.32	3.27 ± 0.29
69	296	1.55 ± 0.10	2.62 ± 0.28	2.95 ± 0.33	1.20 ± 0.11
70	62	1.92 ± 0.12	3.30 ± 0.36	3.41 ± 0.38	2.88 ± 0.24
78	306	1.44 ± 0.09	3.19 ± 0.35	4.83 ± 0.54	3.54 ± 0.31

$$L_{\odot_{max}} = 261.45 \pm 0.07 - (0.15 \pm 0.07) M_r - (0.04 \pm 0.02) M_r^2 . \quad (5)$$

Eq. (5) differs from the one derived by Šimek & McIntosh (1989) who used $\overline{M}_r$ determined for the median durations of the class. Also, the first point in their Fig. 2 for the counts having a duration $T < 1.0\,\mathrm{s}$ which includes a large fraction of underdense echoes is uncertain. Removing this point from the determination of the $L_{\odot_{max}}$ function we have obtained the dependence corresponding to their analysis in the form

$$L_{\odot_{max}} = 261.37 \pm 0.07 - (0.03 \pm 0.12) \overline{M}_r - (0.04 \pm 0.04) \overline{M}_r^2 . \quad (6)$$

The difference between Eqs. (5) and (6) is now explainable due to different definitions of applied radio magnitude.

The skewness of the activity profiles in Fig. 1b–d is evident. The maxima appear after a slower increase of the activity while the descent is characterized by a steeper slope. Class 1 in Fig. 1 suffers from greater fluctuations of points due to their frequent occurrence near the limiting sensitivity of the radar.

For completeness, mean values of the inverse response function of Ondřejov radar resulting from the process of determination of the Geminid cross-section activity are shown in Table 3 for the four groups of meteor echo duration. These values were used in the iterative process to correct the observed hourly rates for the geometry of antenna characteristics and the radiant position on the sky.

Other parameters of the stream, resulting from the calculation of cross-section profiles for echo duration groups presented in Table 1, are shown in Table 4. This table contains variations of the sporadic background activity level, bl, compared to the mean sporadic level over the analyzed years; shower activity level, al, which shows the ratio of recorded shower activity to bl; and the mean relative number of solar activity, R, for December from Waldmeier (1961), for other years this number is published in the Sunspot Bulletin.

4. Background rates and solar activity

Mean echo rates levels of the background were determined by the iterative method mentioned above. Normalized background level coefficients indicating the fraction of the mean value over the whole analyzed period, are presented in Table 4. Table 5 gives, for completeness, the diurnal variations of the mean sporadic background rates in all four echo duration classes.

The influence of solar activity on the observed meteor rates was first examined by Bumba (1949). He analyzed 2441 visually observed meteor events in the period 1844–1943 and concluded that maximum visually observed rates occurred five years after solar activity maximum while their minimum rates appeared two years after minimum solar activity. Lindblad (1975) found a similar dependence from his radar observations of the Perseids from 1953 to 1972 at the Onsala Space Observatory. This correlation model will here be designated as the Bumba-Lindblad model, BL. In later studies Lindblad (1978, 1980) arrived at an inverse correlation between meteor radar hourly rates and the geomagnetic C_p index position within the interplanetary sector structure.

We have studied here a possible correlation of sporadic background levels, (bl in Table 4) with the solar relative number (R in Table 4). Since the duration of the solar cycle in our analyzed period varies from 10 to 12 years, we calculated a sliding mean of consecutive three-year variations of R in an 11-year cycle starting in 1958. The same variation of bl was then correlated with the variation of R. Maximum sporadic meteor activity appears one year after the solar activity maximum. This agreement is expressed by the highest correlation coefficients r shown in Table 1. The correlation for the Bumba-Lindblad model, designated by r_{BL}, valid for a shift of maximum meteor activity by 6 years, is also demonstrated in Table 1. We have found an inverse correlations for all classes of echo durations. No agreement between our model and the BL model has been found.

For a more detail analysis we have used combined data from classes 1 and 3 which contain all observed shower meteors. The procedure of sliding three consecutive years mentioned above was repeated for eleven cases when the background level patterns were consecutively shifted eleven times by one year. The highest serial correlation of both data sets listed in Table 6, $r = 0.81 \pm 0.10$ was found for the shift by 1 ± 1 year with respect to R. Similarly, the highest negative correlation $r = -0.83 \pm 0.09$ fits with a bl vs. R shift of 4–5 years. We may therefore conclude that maximum mean value of the sporadic rates appears 0–2 years after maximum of sunspot number R while minimum sporadic activity appears 4–5 years after maximum R coinciding with the period of minimum solar activity. Our Geminid observations cover solar cycles No 19–22. Histograms of cumulative numbers of sunspots, medium solar flares, large solar flares, and proton flares from satellite data from the same period were published in the Preliminary Report and Forecast of Solar Geophysical Data (1997). It is shown there that two years after the maximum of R and of standard flares there appears a secondary maximum represented by the clear occurrence of large solar flares which corresponds with our maximum of bl. These results show an entirely reverse dependence as compared with the Bumba-Lindblad model.

5. Particle mass distribution and flux

The central part of the shower activity period, the interval $260\overset{\circ}{.}50 \leq L_\odot < 261\overset{\circ}{.}90$, was chosen according to Fig. 1 for analysis of mean diurnal variation of particle mass-distribution.

The diurnal variation of the mass distribution of meteor particles in the stream apparent in Table 7 is not due to the stream character. The mass-distribution indices are here derived from a long-term period when observations at different $L_\odot$ are summed for a particular hour, and the effect of variations of s along the stream is smeared out. We think that this s-variation is of atmospheric origin, combined with an effect of meteor particle penetration angle into the Earth's atmosphere when the same mass of a meteoroid does not produce identical meteor echo duration. Since the observations were carried out mostly from 22 to 07h LT, the number of echoes entering the analysis does not reflect the diurnal variation of observed hourly shower rates of the Geminids. The weighted mean value of s, using a weight

Table 4. Background and activity level coefficients. Normalized background level coefficients, bl, activity level coefficients, al, in four duration classes, and relative sunspot numbers, R, in years of Geminid observations.

Year	Class 1		Class 2		Class 3		Class 4		R
	bl	al	bl	al	bl	al	bl	al	
1958	0.79	4.14	0.89	1.76	0.86	1.40	0.75	3.69	187.6
1959	0.99	6.39	1.16	7.98	1.21	5.93	1.76	8.31	125.0
1960	1.28	4.39	1.39	5.35	1.42	4.23	1.80	3.06	85.6
1961	0.48	8.96	0.81	4.66	0.81	3.30	0.87	12.32	39.9
1962	0.75	7.21	0.96	8.10	0.93	6.05	0.78	9.67	23.2
1963	0.97	7.99	0.89	5.74	0.87	5.89	0.64	4.85	14.9
1964	0.75	6.88	0.77	4.96	0.73	5.05	0.44	2.76	15.1
1965	0.90	9.35	0.92	6.50	0.90	6.14	0.65	5.74	17.0
1966	0.73	12.04	0.95	13.11	0.98	8.93	1.29	13.01	70.4
1967	0.72	8.73	0.86	6.98	0.85	6.20	0.83	13.37	126.4
1968	1.31	7.90	1.00	4.94	1.01	5.34	1.17	5.51	109.8
1969	0.57	10.62	0.67	10.51	0.73	8.41	1.33	19.94	97.9
1971	0.43	9.42	0.63	10.82	0.63	6.53	0.72	13.03	82.2
1973	1.27	6.73	1.07	6.23	1.06	6.55	0.95	4.74	23.3
1974	1.24	7.56	1.19	6.38	1.19	5.96	1.22	5.91	20.5
1975	1.28	6.08	1.31	6.22	1.28	5.73	1.04	10.64	7.8
1976	1.26	10.58	1.03	7.23	1.10	7.49	0.90	7.13	15.3
1977	0.93	8.26	0.88	7.53	0.88	7.71	0.86	11.52	43.2
1978	1.71	7.64	1.32	6.22	1.32	6.75	1.28	3.70	122.7
1980	1.93	5.52	1.97	4.06	1.96	3.83	1.84	4.51	174.4
1981	1.89	6.62	1.56	6.03	1.53	7.34	1.23	7.94	150.1
1982	1.69	7.67	1.58	5.64	1.58	6.01	1.58	9.72	127.0
1984	0.76	9.56	0.83	9.71	0.82	8.62	0.75	14.82	18.7
1985	0.80	6.57	0.79	4.93	0.79	4.28	0.78	6.71	17.3
1986	0.69	9.35	0.73	9.64	0.73	8.24	0.70	9.29	6.8
1987	0.60	10.95	0.81	12.53	0.80	8.68	0.65	10.41	27.1
1989	0.72	9.24	0.63	6.76	0.62	7.72	0.54	10.35	165.6
1990	0.66	10.00	0.62	8.15	0.63	7.92	0.75	10.86	129.7
1991	1.33	5.56	1.14	5.75	1.15	5.76	1.29	6.26	144.4
1992	0.85	9.88	1.04	7.70	1.08	5.68	1.44	8.11	82.6
1993	1.51	6.08	1.10	5.48	1.10	6.95	1.99	7.72	48.9
1994	1.32	7.35	1.19	5.23	1.17	5.47	1.01	5.07	26.2
1995	0.51	27.19	0.49	18.95	0.49	16.96	0.51	10.71	10.0
1996	0.60	7.39	0.77	7.72	0.77	5.61	0.82	8.99	13.3
1997	0.80	7.75	1.03	5.85	1.00	4.62	0.82	9.45	41.2

Table 5. Sporadic background rates. Mean hourly sporadic background rates for specified duration classes versus local time, LT.

LT	0	1	2	3	4	5	6	19	20	21	22	23
class 1	13.4	13.7	14.2	10.9	8.4	7.0	5.4	8.0	9.5	11.5	14.2	13.2
class 2	16.0	15.7	13.7	10.3	8.6	6.3	5.0	4.5	6.7	8.8	14.3	14.7
class 3	17.6	17.1	15.2	11.6	10.0	7.4	6.3	5.0	7.3	10.0	15.2	16.1
class 4	1.6	1.6	1.4	1.4	1.3	1.1	1.3	0.4	0.5	0.7	0.9	1.3

inverse to its standard deviation was found to be 1.48 ± 0.03. Hence, we took this value as the final one for the Geminids. All s values were normalized to the mean value of 1.48 to obtain correcting factors for each hour to determine s unaffected by the diurnal variation.

The mass-distribution index was also investigated along the Earth's path across the stream within $259\overset{\circ}{.}50 \leq L_\odot < 261\overset{\circ}{.}98$ in $\triangle L_\odot = 0\overset{\circ}{.}08$ steps corresponding approximately to two hours. The number of observed echoes depends not only on the shower activity but also on the response function for the relevant hour. So, the total number of cumulative echo rates in each hour within each $\triangle L_\odot$ interval was reduced to one hour rate, N_{hc}. The sums of N_{hc} were then used for the calculation of s according to Eq. (1). To correct s for the diurnal variation, correction factors were calculated as a weighted mean from those in Table 7 using a weight proportional to $\log N_{hc}$. We have chosen

Table 6. Sliding means of R and bl. Three-year sliding means of solar relative numbers, R, and of sporadic activity levels, bl, in an eleven-year cycle versus serial number, starting in 1958. The first number in each row shows the relevant means of data from 1958, 1959, 1960, 1969, 1970, 1971, 1980..., the second column is for years shifted by one year, etc. The following abbreviations have been used: sny – serial number of years, mR – mean R, sdm$R$ – standard deviation of mean R, mbl1 – mean bl for class 1, sdbl1 – standard deviation of mean bl for class 1, mbl3 – mean bl for class 3, sdbl3 – standard deviation of mean bl for class 3.

sny	1	2	3	4	5	6	7	8	9	10	11
mR	118.7	83.1	46.5	20.7	17.7	17.8	27.1	73.5	109.7	139.9	133.5
sdm$R$	13.0	14.3	11.4	2.6	2.9	2.9	7.0	20.4	15.4	10.8	11.5
mbl1	1.205	1.148	0.985	0.870	0.868	0.898	0.880	0.946	0.969	1.083	1.146
sdbl1	0.156	0.162	0.145	0.100	0.076	0.077	0.081	0.131	0.150	0.168	0.168
mbl3	1.205	1.171	1.003	0.891	0.889	0.924	0.933	0.930	0.897	1.014	1.128
sdbl3	0.119	0.105	0.107	0.066	0.063	0.058	0.060	0.075	0.092	0.142	0.136

Table 7. The mass-distribution index for the central part of the Geminids. Mean mass-distribution index s for Geminids having echo durations $T \geq 0.4$ s summarized over all years of the Geminid observations, in the central part of the shower activity corresponding to the interval $260^\circ\!.50 \leq L_\odot < 261^\circ\!.9$, relevant correction factors for the elimination of its diurnal variation, number of echoes entering the analysis and the range of the linear part of $\log N_c$ vs. $\log T$ curve. Values of s represent their mean diurnal variation derived from shower echo counts.

Local time, LT	s	correction for the mean	Number of echoes	Linear part of echo duration interval of the sample [s]
00	1.44 ± 0.01	1.024 ± 0.010	5319	0.4–2.0
01	1.36 ± 0.01	1.087 ± 0.011	5914	0.4–2.0
02	1.38 ± 0.01	1.069 ± 0.010	6352	0.4–2.0
03	1.47 ± 0.01	1.004 ± 0.011	6318	0.4–1.6
04	1.43 ± 0.01	1.033 ± 0.011	4568	0.4–1.6
05	1.44 ± 0.01	1.030 ± 0.010	2841	0.4–2.0
06	1.50 ± 0.01	0.987 ± 0.011	2263	0.4–2.0
07	1.52 ± 0.01	0.973 ± 0.010	798	0.4–2.4
08	1.62 ± 0.06	0.916 ± 0.020	41	0.4–1.6
09	1.68 ± 0.11	0.877 ± 0.040	20	0.4–2.0
20	1.69 ± 0.06	0.875 ± 0.019	176	0.4–2.0
21	1.69 ± 0.02	0.875 ± 0.020	485	0.4–3.5
22	1.58 ± 0.01	0.934 ± 0.009	1579	0.4–2.9
23	1.47 ± 0.01	1.008 ± 0.010	3578	0.4–2.0
Weighted mean	1.48 ± 0.02	Total number	40251	

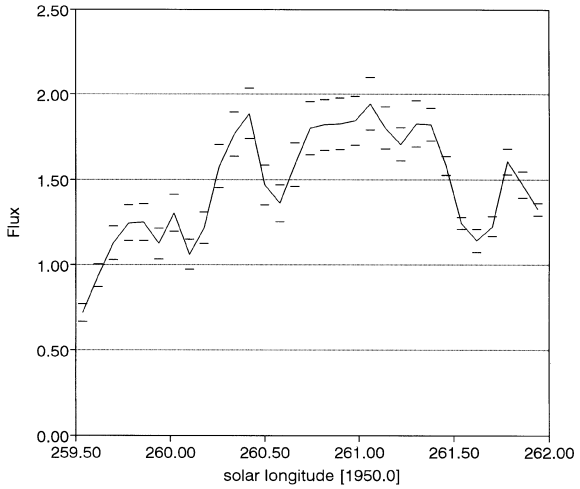

Fig. 2. The 1958–1997 Geminid mean flux in the central part of shower activity as a function of solar longitude, $L_\odot$ (1950.0). Flux is expressed in units of $10^{-12}\,\mathrm{m}^{-2}\,\mathrm{s}^{-1}$.

this weighting factor even though we are aware that it may not be strictly correct. The result is presented in Table 8. Another possibility of s determination is its simultaneous computation with the flux, Θ_{m_0}, as it was mentioned in Sect. 2. Since this approach includes the information concerning the mutual positions of the shower radiant and the antenna pattern, it need not be corrected for diurnal changes. Results of simultaneous flux and s determination are shown in Fig. 2 and 3 and are also included in Table 8. We can see from it that values of s computed together with fluxes are somewhat higher than s following from Eq. (1). This can partly be attributed to the fact that the method of flux determination takes into consideration the different collecting area within the echo plane of echoes having different duration. This leads to underestimated rates of short-duration echoes and consequently lower values of s when using Eq. (1). However, the trends of both s-curves are the same. The flux behaviour is more complicated than the behaviour of s. The maximum value of the flux has been found to occur between $261^\circ\!.02 \leq L_\odot < 261^\circ\!.10$

Table 8. Mass-distribution indices and flux. The mass-distribution index across the stream corrected for diurnal variation, and the mass-distribution index and flux following from simultaneous determination of both quantities. The designations used: ne – number of echoes, lpedi – linear part of echo duration interval of the sample in seconds. The flux Θ_{m_0} is expressed in units of $10^{-12}\,\mathrm{m}^{-2}\,\mathrm{s}^{-1}$.

$L_\odot$-interval	s following from (1)	ne	lpedi	s and Θ_{m_0} following from (3) s	Θ_{m_0}
259.50–259.58	1.67 ± 0.01	299	0.5–2.0	1.76 ± 0.06	0.72 ± 0.05
259.58–259.66	1.71 ± 0.03	464	0.4–1.3	1.98 ± 0.06	0.94 ± 0.07
259.66–259.74	1.79 ± 0.02	395	0.7–2.9	1.88 ± 0.07	1.13 ± 0.10
259.74–259.82	1.82 ± 0.02	579	0.4–1.6	2.02 ± 0.07	1.25 ± 0.11
259.82–259.90	1.80 ± 0.02	635	0.4–2.4	1.95 ± 0.07	1.25 ± 0.11
259.90–259.98	1.80 ± 0.02	571	0.4–2.4	1.95 ± 0.07	1.13 ± 0.09
259.98–260.06	1.58 ± 0.02	596	0.4–1.6	1.82 ± 0.07	1.31 ± 0.11
260.06–260.14	1.54 ± 0.02	617	0.4–2.0	1.72 ± 0.07	1.06 ± 0.09
260.14–260.22	1.62 ± 0.02	775	0.4–2.0	1.76 ± 0.06	1.22 ± 0.09
260.22–260.30	1.65 ± 0.02	884	0.4–2.0	1.78 ± 0.07	1.58 ± 0.13
260.30–260.38	1.64 ± 0.02	901	0.4–2.0	1.75 ± 0.06	1.77 ± 0.13
260.38–260.46	1.60 ± 0.02	992	0.4–2.0	1.72 ± 0.06	1.89 ± 0.15
260.46–260.54	1.59 ± 0.02	903	0.4–2.0	1.66 ± 0.07	1.47 ± 0.12
260.54–260.62	1.64 ± 0.02	836	0.4–2.0	1.74 ± 0.07	1.36 ± 0.11
260.62–260.70	1.58 ± 0.02	995	0.4–2.4	1.66 ± 0.07	1.59 ± 0.13
260.70–260.78	1.56 ± 0.02	1104	0.4–2.4	1.63 ± 0.07	1.80 ± 0.16
260.78–260.86	1.54 ± 0.02	1067	0.4–2.0	1.62 ± 0.07	1.82 ± 0.15
260.86–260.94	1.52 ± 0.02	1009	0.4–2.4	1.66 ± 0.07	1.83 ± 0.15
260.94–261.02	1.47 ± 0.02	1061	0.4–2.4	1.57 ± 0.07	1.85 ± 0.14
261.02–261.10	1.46 ± 0.02	1022	0.4–2.0	1.57 ± 0.07	1.95 ± 0.15
261.10–261.18	1.42 ± 0.02	1137	0.4–2.0	1.49 ± 0.07	1.80 ± 0.12
261.18–261.26	1.47 ± 0.02	1149	0.4–2.9	1.46 ± 0.06	1.71 ± 0.10
261.26–261.34	1.44 ± 0.01	1130	0.4–2.4	1.50 ± 0.07	1.83 ± 0.13
261.34–261.42	1.43 ± 0.02	1200	0.4–2.4	1.43 ± 0.06	1.82 ± 0.10
261.42–261.50	1.45 ± 0.02	1003	0.7–2.9	1.38 ± 0.05	1.58 ± 0.06
261.50–261.58	1.40 ± 0.01	906	0.4–2.9	1.33 ± 0.05	1.24 ± 0.04
261.58–261.66	1.39 ± 0.01	784	0.4–2.0	1.41 ± 0.07	1.14 ± 0.07
261.66–261.74	1.39 ± 0.01	779	0.4–1.6	1.38 ± 0.06	1.23 ± 0.06
261.74–261.82	1.41 ± 0.02	857	0.4–2.4	1.41 ± 0.06	1.61 ± 0.07
261.82–261.90	1.44 ± 0.01	691	0.4–2.0	1.42 ± 0.06	1.47 ± 0.08
261.90–261.98	1.36 ± 0.02	575	0.4–2.4	1.31 ± 0.06	1.33 ± 0.04

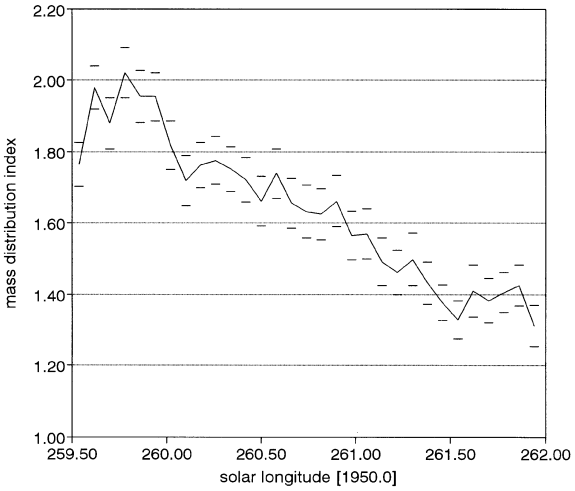

Fig. 3. The same as in Fig. 2 but for the mass-distribution index, s.

while the minimum value of s occurred at the edge of the whole activity interval (see Table 8).

Profiles of the stream in Fig. 1a,b and d should be taken into consideration when discussing the variation of s across the stream from Table 8. The character of the mass-distribution indices gives a picture of the particle distribution without a dependence on the absolute echo count number. Therefore, no agreement of the extreme value of s with the position of shower activity peak is expected. So we conclude that the higher values of s at the beginning of the analyzed interval are a consequence of low rates of long-duration echoes (Fig. 1d) in $259\overset{\circ}{.}5 \leq L_\odot \leq 260\overset{\circ}{.}9$. Similarly, lower values of s at the end of the interval confirm the lack of faint particles in this part of the stream in accordance with Fig. 1a. Such a feature has also been found by Brown et al. (1998) from 1996 observations. Activity profiles in Figs. 1a,b and d combined with the distribution of the index s in Table 8 yield an image of the stream as a complex of gradually changing distribution of the dominant mass of the particles encountering the Earth.

Table 9. Variation of sporadic background s. Diurnal variation of the mass-distribution index s of the sporadic background. The designations used: mhr – mean hourly rate in the sample, lpedi – linear part of echo duration interval of the sample in seconds.

Time, LT	s	mhr	lpedi
00	2.19 ± 0.01	28.7	0.5–2.9
01	2.16 ± 0.01	39.4	0.4–2.9
02	2.19 ± 0.02	39.8	0.4–3.5
03	2.29 ± 0.02	39.7	0.4–3.5
04	2.16 ± 0.01	15.2	0.7–3.5
05	2.12 ± 0.01	12.7	0.7–5.0
06	2.03 ± 0.02	10.2	0.7–3.5
07	1.91 ± 0.01	6.9	0.9–6.0
08	1.79 ± 0.02	5.7	0.5–10.0
09	1.97 ± 0.04	7.9	0.5–10.0
10	1.97 ± 0.06	9.5	0.4–6.0
11	1.95 ± 0.03	12.2	0.4–5.0
12	2.40 ± 0.07	8.6	0.5–2.9
13	2.18 ± 0.04	13.2	0.4–17.0
14	1.99 ± 0.05	6.0	0.7–6.0
15	2.38 ± 0.13	11.9	0.4–6.0
16	2.47 ± 0.09	7.4	0.4–5.0
17	2.54 ± 0.10	7.3	0.4–4.2
18	2.48 ± 0.36	11.1	0.4–7.5
19	2.95 ± 0.07	11.7	0.4–10.0
20	2.75 ± 0.04	17.6	0.4–17.0
21	2.67 ± 0.03	21.7	0.4–13.0
22	2.46 ± 0.01	26.6	0.4–5.0
23	2.35 ± 0.01	35.4	0.4–4.2

A similar analysis was carried out for the diurnal variation of the mass-distribution index of sporadic meteors appearing in the periods $256\overset{\circ}{.}00 \leq L_\odot \leq 258\overset{\circ}{.}00$ and $263\overset{\circ}{.}00 \leq L_\odot \leq 265\overset{\circ}{.}00$. The result is shown in Table 9. The mean value of s over a 24-hour period was found to be $s = 2.26 \pm 0.06$, the mean s in sunlit hours is 2.10 ± 0.08, and during the darkness period at meteor height of 93 km, $s = 2.38 \pm 0.07$, while within the Geminid occurrence fraction of the day between 20h and 10h LT, $s = 2.17 \pm 0.07$ which is in agreement with the generally accepted value for the sporadic background.

6. Conclusions

We have analyzed radar meteor records from 35 Geminid campaigns carried out from 1958 to 1997. In total, approximately 120,000 overdense echoes of shower and sporadic meteors having durations $T \geq 0.4$ s were recorded. Such a large amount of data enabled the investigation of shower activity profiles across the stream in four echo duration categories. It has been found that the widths of the stream profiles and the degree of skewness are dependent on particle size. The skewness of the profiles in all classes except that for $0.4 \leq T < 1$ s indicates a slow rise to the peak followed by a more rapid decrease. In combination with the course of the mass-distribution index across the stream showing minimum values at the descending parts of the activity profiles, this suggests a continuous change of the particle number distribution across the stream depending on particle size. The gradually changing position of peaks in activity profiles expressed by Eq. (5) is in agreement with this. The change is probably due to the Poynting-Robertson effect which pushes small particles back to the region of inner orbits of the stream (Plavcová 1962, Šimek 1973). The influx of larger particles from the Geminid stream peaking later than the smaller particles was also pointed out by Millman & McIntosh (1963) and McIntosh (1966). Levels of shower activity demonstrate considerable variation along the stream orbit proving its inhomogeneity. This is also confirmed by the course of the flux curve reaching its maximum within the interval $261\overset{\circ}{.}02 \leq L_\odot < 261\overset{\circ}{.}10$. The maximum value we have found reached $\Theta_{m_0} = (1.95 \pm 0.15) \times 10^{-12}\ \mathrm{m}^{-2}\ \mathrm{s}^{-1}$.

Attention was also given to the dependence of sporadic meteor radar echo rates on the phase of the solar cycle. Contrary to Bumba (1949) and Lindblad (1975) we have found a high correlation ($r = 0.96 \pm 0.02$ for class 4), for radar meteor activity delayed by 1 ± 1 year after the maximum of the solar cycle expressed in relative number, R, representing the occurrence of sunspots.

Acknowledgements. The authors appreciate Dr. L. Křivský from their Institute for his comments concerning the influence of solar activity. The authors are also grateful to Dr. B. A. McIntosh for the correction of the wording of the article. This work was supported by the key project K1-003-601 and the grant No 205/96/1197 of the Grant Agency of Czech Republic.

References

Baggaley W.J., 1972, MNRAS 159, 203
Brown P., Hocking W.K., Jones J., Rendtel J., 1998, MNRAS 295, 847
Bumba V., 1949, Bull Astron. Inst. Czechosl. 1, 93
Fox K., Williams I.P., Hughes D.W., 1983, MNRAS 205, 1155
Hajduk A., McIntosh B.A., Šimek M., 1974, Bull. Astron. Inst. Czechosl 25, 305
Jacchia L.G., Verniani F., Briggs R.E., 1965, Research in Space Science (Special Report 175; Smithson. Astrophys. Obs.), April 1965
Jones J., McIntosh B.A., Šimek M., 1990, J. Atmos. Terr. Phys. 52, 253
Kaiser T.R., 1955, In: Kaiser T.R. (ed.) Meteors. Pergamon Press, London, 119
Kashcheev B.L., Lebedinets V.N., Lagutin M.F., 1967, Rezul'taty Issled. IGY, Issled. Meteorov No. 2
Lindblad B.A., 1975, Meteor radar rates and the Solar Cycle. Presented at IAU Colloquium No. 31 on Interplanetary Dust and Zodiacal Light, Heidelberg
Lindblad B.A., 1978, Nat 273, 732
Lindblad B.A., 1980, In: Halliday I., McIntosh B.A. (eds.) Solid Particles in the Solar System. 105
McIntosh B.A., 1966, Canad. J. Phys 44, 2729
McIntosh B.A., Šimek M., 1980, Bull. Astron. Inst. Czechosl. 31, 39
McKinley D.W.R., 1961, Meteor Science and Engineering. McGraw-Hill, New York
Millman P.M., McIntosh B.A., 1963, Smithsonian Contr. Astrophys. 7, 45
Pecina P., 1982, Bull. Astron. Inst. Czechosl. 33, 1
Plavcová Z., 1962, Bull. Astron. Inst. Czechosl. 13, 176

Plavcová Z., 1965, Bull. Astron. Inst. Czechosl. 16, 127
Preliminary Report and Forecast of Solar Geophysical Data, Boulder, 1997, No 1136
Spurný P., 1993, In: Štohl J., Williams I.P. (eds.) Meteoroids and their parent bodies. Astronomical Institute, Slovak Academy of Sciences, Bratislava, 193
Šimek M., 1973, Bull. Astron. Inst. Czechosl. 24, 213
Šimek M., 1985, Bull. Astron. Inst. Czechosl. 36, 270
Šimek M., 1987, Bull. Astron. Inst. Czechosl. 38, 80
Šimek M., McIntosh B.A., 1986, Bull. Astron. Inst. Czechosl. 37, 146
Šimek M., McIntosh B.A., 1989, Bull. Astron. Inst. Czechosl. 40, 288
Sunspot Bulletin: Sunspot Index Data Center Brussels
Waldmeier M., 1961, The Sunspot-Activity in the Years 1610–1960. Zurich, Schulthess & Co AG
Whipple F.L., 1983. IAU Circ. No 3881
Znojil V., Šimek M., Grygar J., Hollan J., 1981, Bull. Astron. Inst. Czechosl. 32, 1